Functional connectivity with the retrosplenial cortex predicts cognitive aging in rats

Jessica A. Ash[a,1,2], Hanbing Lu[b,2], Lisa R. Taxier[a], Jeffrey M. Long[a], Yihong Yang[b], Elliot A. Stein[b], and Peter R. Rapp[a,3]

[a]Laboratory of Behavioral Neuroscience, National Institute on Aging, Biomedical Research Center, National Institutes of Health (NIH), Baltimore, MD 21224; and [b]Neuroimaging Research Branch, National Institute on Drug Abuse, Biomedical Research Center, NIH, Baltimore, MD 21224

Edited by Marcus E. Raichle, Washington University in St. Louis, St. Louis, MO, and approved September 13, 2016 (received for review December 23, 2015)

Changes in the functional connectivity (FC) of large-scale brain networks are a prominent feature of brain aging, but defining their relationship to variability along the continuum of normal and pathological cognitive outcomes has proved challenging. Here we took advantage of a well-characterized rat model that displays substantial individual differences in hippocampal memory during aging, uncontaminated by slowly progressive, spontaneous neurodegenerative disease. By this approach, we aimed to interrogate the underlying neural network substrates that mediate aging as a uniquely permissive condition and the primary risk for neurodegeneration. Using resting state (rs) blood oxygenation level-dependent fMRI and a restrosplenial/posterior cingulate cortex seed, aged rats demonstrated a large-scale network that had a spatial distribution similar to the default mode network (DMN) in humans, consistent with earlier findings in younger animals. Between-group whole brain contrasts revealed that aged subjects with documented deficits in memory (aged impaired) displayed widespread reductions in cortical FC, prominently including many areas outside the DMN, relative to both young adults (Y) and aged rats with preserved memory (aged unimpaired, AU). Whereas functional connectivity was relatively preserved in AU rats, they exhibited a qualitatively distinct network signature, comprising the loss of an anticorrelated network observed in Y adults. Together the findings demonstrate that changes in rs-FC are specifically coupled to variability in the cognitive outcome of aging, and that successful neurocognitive aging is associated with adaptive remodeling, not simply the persistence of youthful network dynamics.

resting-state fMRI | default mode network | functional connectivity | neurocognitive aging | rat model

Functional MRI (fMRI) has revealed a number of functionally interconnected brain networks. One prominent example, termed the default mode network (DMN), shows prominent temporally coherent activity under wakeful, spontaneous, and undirected conditions (i.e., "resting"), and decreased coherence in response to active cognitive engagement (1–3). Functional connectivity (FC) assessed from the blood oxygenation level-dependent (BOLD) signal provides a measure of these coincident fluctuations across brain areas (2, 4), where positive correlations are thought to reflect simultaneous neuronal activity between regions, and negative or "anticorrelations" arise from inverse, antiphase fluctuations. In this way, resting-state FC (rs-FC) maps the temporal and spatial organization of large-scale neural network dynamics.

Recent studies indicate that variability in DMN FC is linked to individual differences in cognition and behavior (e.g., refs. 5 and 6), including differential trajectories of cognitive aging. For example, the strength of FC between anterior and posterior components of the DMN across the lifespan is directly related to performance on tasks measuring executive function, memory, and processing speed (7). During normal aging (i.e., in the absence of neurodegenerative disease), individuals with marked reductions in DMN connectivity also show significant cognitive decline relative to age-matched subjects with stronger FC (7–9). This relationship appears particularly robust for associative memory (10–12), where the strength of temporal coherence between the hippocampus and posteriomedial areas of the DMN (i.e., the precuneus and cingulate cortex) predicts face–name memory performance (12). Although rs-dynamics are also disrupted in a number of other conditions (for a review, see ref. 13), the significant insight into aging has been that, superimposed on the vulnerability of individual brain regions important for normal function, cognitive decline may arise, in part, as an emergent property of aberrant network organization.

The degree of disruption in DMN FC also varies along the continuum of advanced aging phenotypes, with a more extensive loss of connectivity seen in Alzheimer's disease (AD) relative to normal aging (14–16). Indeed, considerable interest has centered on DMN integrity as a potential early biomarker for AD (14). The underlying mechanisms of disconnection are unclear but may be linked to amyloid deposition, which preferentially targets DMN hubs in AD patients (17, 18). This pattern is not specific to AD, however, as a substantial proportion of cognitively normal older individuals also exhibit reduced FC in the DMN in association with amyloid burden in these same cortical hubs (19–22). A significant additional challenge is that, because the preclinical course of AD is protracted and likely extends over more than a decade (23), it is unknown what proportion of clinically normal individuals with significant amyloid burden is already on the pathophysiological trajectory of disease. Disentangling the contribution of normal and pathological aging to reported changes in rs-activity has therefore proved difficult on the basis of human studies alone.

The neuroanatomical distribution of DMN rs-activity observed in humans is at least partly conserved in rats (24, 25) and nonhuman primates (26–29). Because common laboratory animal species fail to spontaneously develop neuropathological hallmarks of human aging (e.g., widespread neuron loss, amyloid deposition, tauopathy, and cerebrovascular disease), research in these models

Significance

Neural network dynamics thought to play a key role in cognition are substantially disrupted in both normal and pathological aging. Using a rat model, here we aimed to define the effects of aging on the integrity of cortical resting state functional connectivity distinct from the potential contribution of neurodegenerative disease. The findings highlight that disrupted circuit connectivity with the retrosplenial/posterior cingulate cortex is coupled with variability in memory function during aging, and that adaptive plasticity in the aged brain appears to contribute to successful cognitive aging. The development of interventions that promote neuroadaptive network plasticity is a potentially valuable alternative to strategies currently under investigation, toward bending the trajectory of aging away from neurodegeneration.

Author contributions: J.A.A., H.L., Y.Y., E.A.S., and P.R.R. designed research; J.A.A., H.L., L.R.T., and J.M.L. performed research; J.A.A., H.L., and L.R.T. analyzed data; Y.Y., E.A.S., and P.R.R. provided feedback on all aspects of research from design to writing; and J.A.A., Y.Y., E.A.S., and P.R.R. wrote the paper.

The authors declare no conflict of interest.

This article is a PNAS Direct Submission.

[1]Present address: SomaLogic, Inc., 2945 Wilderness Pl., Boulder, CO 20301.

[2]J.A.A. and H.L. contributed equally to this work.

[3]To whom correspondence should be addressed. Email: rappp@mail.nih.gov.

This article contains supporting information online at www.pnas.org/lookup/suppl/doi:10.1073/pnas.1525309113/-/DCSupplemental.

can provide a window on brain aging uncontaminated by frank neurodegenerative disease. Here we took advantage of a well-characterized rat model optimized for detecting individual differences in the neurocognitive outcome of aging (for a review, see ref. 30). As a starting point, our initial aim was to determine whether aged rats, like young animals (24, 25, 31–33), display coherent rs-FC in the rodent homolog of the DMN, as defined by placing a seed in a key DMN hub, the retrosplenial/posterior cingulate cortex (RSC/PCC). Second, brain-wide rs-FC examined in this context allowed us to test whether changes in cortical network dynamics are specifically coupled with age-related cognitive decline or instead reflect an obligatory outcome of chronological aging. Aging comprises the single greatest risk for AD (34), and considerable research suggests that the neurobiological setting of cognitive aging represents a key permissive condition for the development of neurodegenerative disease (35). Thus, combined with evidence that changes in network activity might directly contribute to neuronal vulnerability and pathogenesis, our experiments aimed to shed light on the critical interface of brain aging and neurodegeneration (36), when the prospects for disease modifying intervention are greatest.

Results

Individual Differences in Hippocampal Memory in Aged Rats. Spatial learning in the Morris water maze (MWM) provided a framework for evaluating the functional significance of age-related changes in rs-FC. Before imaging, young adult (6–7 mo) and aged (24–25 mo) male Long–Evans rats were tested on a standardized spatial version of the task that reveals reliable individual differences in hippocampal integrity and the cognitive outcome of aging (37). Learning and memory for the hidden platform location were assessed using a learning index (LI) score, calculated for each animal as the weighted average proximity to the escape location (in centimeters) during several probe trials interleaved throughout an 8-d protocol (37). By this measure, low values reflect searching near the platform position and better memory. LI scores for young (Y) rats (n = 12) were comparable to previous research (for e.g., ref. 38), ranging from 147 to 221 (mean ± SEM = 187 ± 8.66, n = 12). Adopting an approach validated in earlier research in this model, aged animals were characterized as aged unimpaired (AU) if they performed comparable to normative population values for young rats (range for AU = 165–230, mean ± SEM = 205 ± 5.31, n = 12), and aged impaired (AI) if they scored worse than 250 (range = 251–330, mean ± SEM = 277 ± 7.01, n = 12). The distribution of scores for individual rats is shown in Fig. 1.

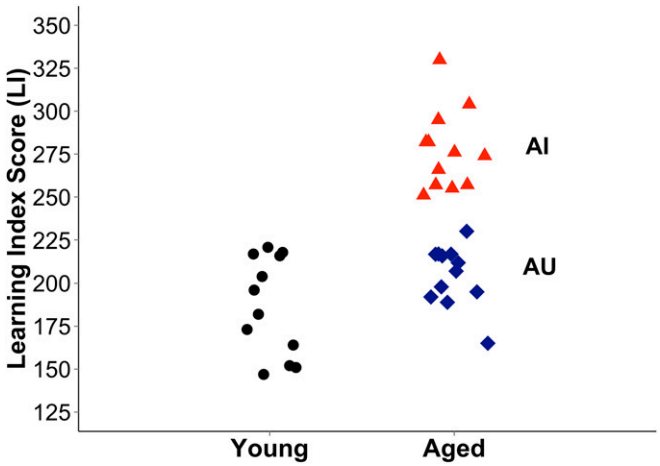

Fig. 1. LI scores from MWM performance for individual Y (n = 12, black circle), AU (n = 12, blue diamond), and AI (n = 12, red triangle) rats. Aged animals with scores comparable to values for young rats in this model were classified as AU, whereas aged animals with scores outside the normative Y distribution were classified as AI, reflecting less accurate searching in the vicinity of the escape platform across probe trials.

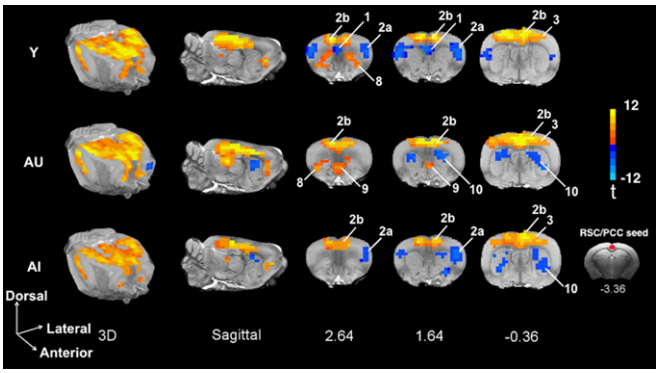

Fig. 2. Maps of mean FC for Y, AU, and AI rats based on a region of interest analysis using a seed (*Bottom Right*) in the RSC/PCC. In all groups, the maps (*Left*) reveal a network qualitatively similar to the rodent DMN homolog described previously in young rats and other species (*Results*). The 2D slices (*Right*) illustrate the distribution of both positive (red-yellow) and anticorrelated (blue) networks at three anterior–posterior levels in the Y, AU, and AI groups (Fig. 4). All $P < 0.05$ are corrected for multiple comparisons. Key: 1, cingulate cortex; 2a, insular cortex; 2b, motor cortex; 3, somatosensory cortex; 8, orbitofrontal cortex; 9, infralimbic/prelimbic cortex; and 10, caudate putamen. Coordinates represent distance relative to bregma (in millimeters).

Region of Interest Analysis: The DMN Is Present in the Aged Rat Brain. Structural and rs-fMRI data were acquired approximately 1 mo after behavioral testing, during which rats acclimated to colony space in close proximity to the neuroimaging facilities. Twilight anesthesia was maintained throughout rs-scanning using a low concentration of isoflurane (iso) (0.5–0.75%) and s.c. dexmedetomidine (dex) (0.01 mg/kg/h), adopted from a protocol previously validated to preserve rs-FC dynamics in the rat (24). Animals were selected for the present experiment such that average body weight did not differ as a function of age or cognitive status [$F(2,33)$ = 0.728, P = 0.491; Fig. S1]. Body temperature (37.2 ± 0.5 °C) was controlled, and oxygen saturation (maintained at 95–100%) did not differ across groups (Kruskal–Wallis test, H = 2.056, P = 0.358). Heart rate was also comparable between AU and AI rats (Mann–Whitney test, U = 57.5, P = 0.895; Fig. S2). Although there was a trend toward an anesthesia effect on respiration rate in AI vs. AU (Mann–Whitney test, U = 38, P = 0.053; Fig. S3), control analyses suggest a generalized change in neurovascular coupling is unlikely to account for altered FC observed among the aged subgroups (see piriform cortex analysis, below).

Our initial aim was to extend our earlier demonstration of the DMN in young rats to aged animals (24), defined by placing a seed in the RSC/PCC (Fig. 2, *Bottom Right*) and calculating the correlation coefficient for the mean time series of the seed with the corresponding values for every other voxel in the brain (*SI Materials and Methods*). Mean FC maps with the RSC/PCC seed for each group (Fig. 2, 3D-rendered maps on *Left*) revealed a distributed network of brain regions consistent with previous findings in young rats (24), overlapping key homologous components of the DMN in nonhuman primates (26–29) and humans (2, 3). Areas displaying temporally coherent, bilateral activity included orbitofrontal and prelimbic divisions of the prefrontal cortex, anterior cingulate cortex, dorsal hippocampus, retrosplenial cortex, posterior parietal cortex (including the medial secondary visual area considered part of the rat parietal cortex) (39), and primary/secondary auditory and temporal association cortices. Consistent with earlier descriptions in humans (40, 41) and rats (24, 25), Y animals also exhibited temporally anticorrelated or inverse activity patterns between the RSC/PCC seed and both the insula and anterior cingulate cortex (Fig. 2, 2D slices, *Top* row). Aged rats displayed an anticorrelated network as well, but with a different anatomical localization involving the caudate putamen (Fig. 2, 2D slices, *Middle* and *Bottom* rows). Finally, similar to work using other midline cortical seeds (25), in all groups, the distribution of brain

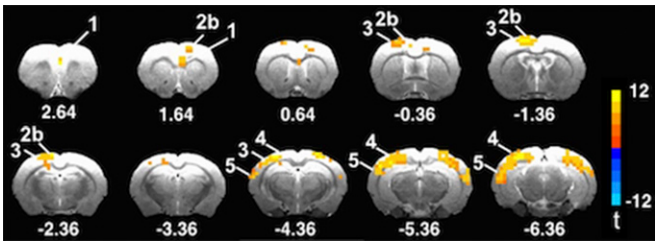

Fig. 3. A significant main effect of group revealed differences in FC with the RSC/PCC ($P < 0.05$, corrected for multiple comparisons) of five clusters: 1, cingulate cortex; 2b, motor cortex; 3, somatosensory cortex; 4, posterior parietal cortex/secondary visual cortex; and 5, dorsal auditory cortex/temporal association cortex. Coordinates represent distance relative to bregma (in milliliters).

regions showing significant coherence extended beyond areas generally considered core components of the primate DMN, with less anterior/posterior segregation, including posterior somatosensory and motor cortices and dorsal aspects of the thalamus.

RSC/PCC FC Is Widely Disrupted Selectively in Aged Rats with Cognitive Impairment. Next, we conducted an unbiased, whole brain survey to test whether rs-cortical network interaction with the RSC/PCC is altered in the aged rat. Mean FC maps were compared across Y, AU, and AI groups using a one-way ANOVA. The results revealed a significant main effect of group [$F(2,33) = 5.31$, $P < 0.05$; Fig. 3]; subsequent between-group contrasts confirmed that age-related changes in RSC/PCC rs-FC were predominantly restricted to aged rats with memory impairment (AI). Aside from the important exceptions discussed below, involving a frontoinsular area, contrasts between Y and AU revealed no significant differences (Fig. 4*A*, $P <$ 0.05 cluster corrected, $t \geq 2.82$), suggesting that rs-FC with the RSC/PCC is relatively preserved in aged rats with intact cognitive function. In contrast, AI animals showed significant and widespread reductions in FC compared with Y rats, spanning primary and secondary motor and somatosensory areas, as well as uni- and multimodal association areas (i.e., posterior parietal cortex and secondary visual cortex, and dorsal auditory cortex and temporal association cortex), and the dorsal hippocampus (Fig. 4*B*, $P < 0.05$ cluster corrected, $t \geq 2.82$). A qualitatively similar pattern of reduced connectivity was also observed when comparing AI and AU rats, although in this case differences were somewhat less spatially extensive (Fig. 4*C*, $P < 0.05$ cluster corrected, $t \geq 2.82$). Notably, the distribution of changes observed in AI rats included many regions not considered major components of the DMN, and conversely, not all DMN hubs were prominently affected. Together the findings suggest that decline in cortical network integrity is not an inevitable consequence of aging, and instead that cortical FC with the RSC/PCC is widely disrupted specifically in association with cognitive impairment.

In addition to a preservation of connectivity among regions that showed positive coherence, AU rats displayed a reduction of rs-FC in a network that exhibited anticorrelated activity with the RSC/PCC seed in Y rats (Fig. 2, 2D slices). Specifically, AU rats showed reduced connectivity between the RSC/PCC seed and right frontoinsular cortex relative to Y rats (Fig. 4*A*, where the loss of the anticorrelated FC is represented as a net positive shift). A growing body of evidence suggests that successful cognitive outcomes in aging arise from active neurobiological adaption (42), perhaps comprising the substrates of cognitive resilience and reserve. Here, the affected network in AU rats involved frontoinsular circuitry implicated in switching between the DMN and executive control networks (41). In contrast, there was no significant change in activity across anticorrelated networks comparing AI to Y rats (Fig. 4*B*).

A parallel control analysis tested the specificity of FC changes in aging, using the piriform cortex (PC) as a seed region to map connectivity. The PC is a unimodal olfactory region in rodents that is reportedly relatively preserved in aged rats (43). Here, in contrast to

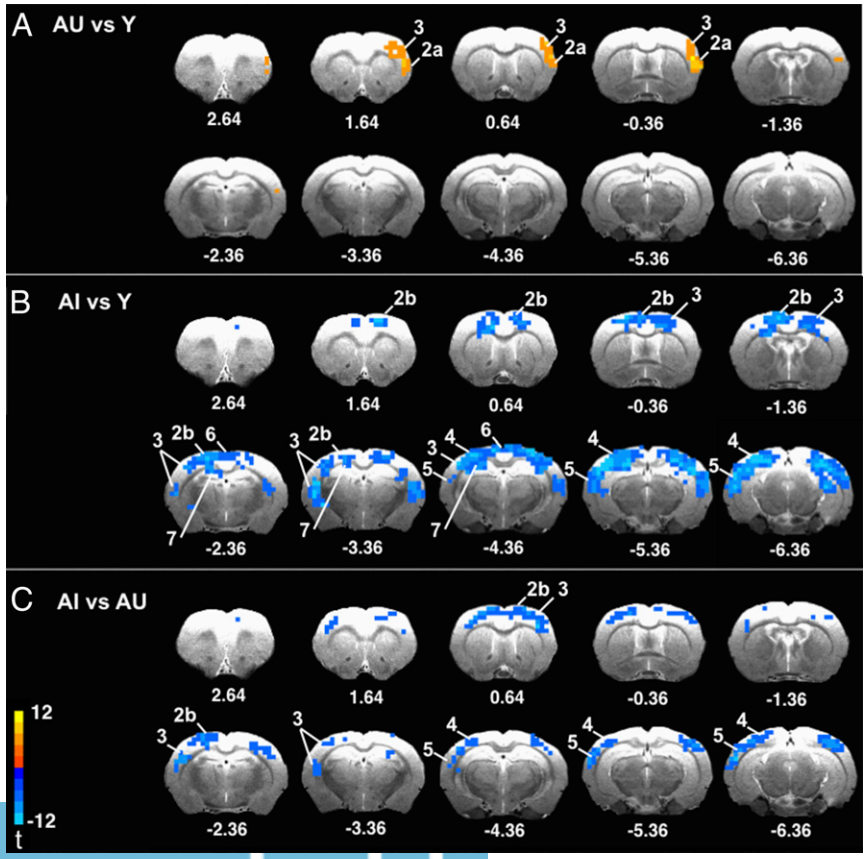

Fig. 4. Contrast maps plotting the distribution of significant differences in FC with the RSC/PCC ($P <$ 0.05, corrected for multiple comparisons). (*A*) AU vs. Y. (*B*) AI vs. Y. (*C*) AI vs. AU. Whereas AI rats showed prominent reductions in connectivity compared with Y rats, distributed across both DMN and non-DMN areas, AU animals showed relatively preserved positive FC, together with a loss of an anticorrelated network observed in Y. Key: 2a, insular cortex; 2b, motor cortex; 3, somatosensory cortex; 4, posterior parietal cortex/secondary visual cortex; 5, dorsal auditory cortex/temporal association cortex; 6, retrosplenial cortex; and 7, hippocampus. Coordinates represent distance relative to bregma (in milliliters).

RSC/PCC connectivity (Fig. 3), the main effect of group showed no significant differences in rs-FC using a cluster corrected $P \leq 0.05$ [$F(2,33) = 1.85$, $P > 0.05$; Fig. S4], suggesting that the effects of aging on functional connectivity are network specific rather than a ubiquitous consequence of brain aging. These findings also count against the possibility that age-related changes in general physiology lead to altered neurovascular coupling and diffuse, nonspecific change in BOLD signal.

Lastly, we used a linear regression model to determine whether LI scores for individual rats predict FC strength. When all animals were included in the analysis, the results indicated that higher LI scores (reflecting poor spatial memory) were significantly associated with reduced FC (Fig. 5*A*, $r = -0.44$, $P = 0.007$), involving several regions affected in AI rats (e.g., sensorimotor cortex, posterior parietal/secondary visual cortex, and dorsal auditory/temporal association cortex; Fig. 5*B*). This association, however, may predominantly reflect the observed between-group differences in behavior and FC. Consistent with this possibility, none of the correlations remained statistically significant when the Y, AU, and AI groups were considered individually (all P values >0.05). The number of subjects available for the latter analyses was limited ($n = 12$ per group), and studies in larger samples will be needed to confirm whether there is a linear relationship between individual differences in hippocampus-dependent spatial memory and RSC/PCC rs-FC in aged rats. Nonetheless, whereas research in preclinical animal models has focused on distinguishing the role of isolated brain regions, like the hippocampus, the current findings are consistent with the idea that cognitive aging additionally reflects more widely distributed cortical network disruptions.

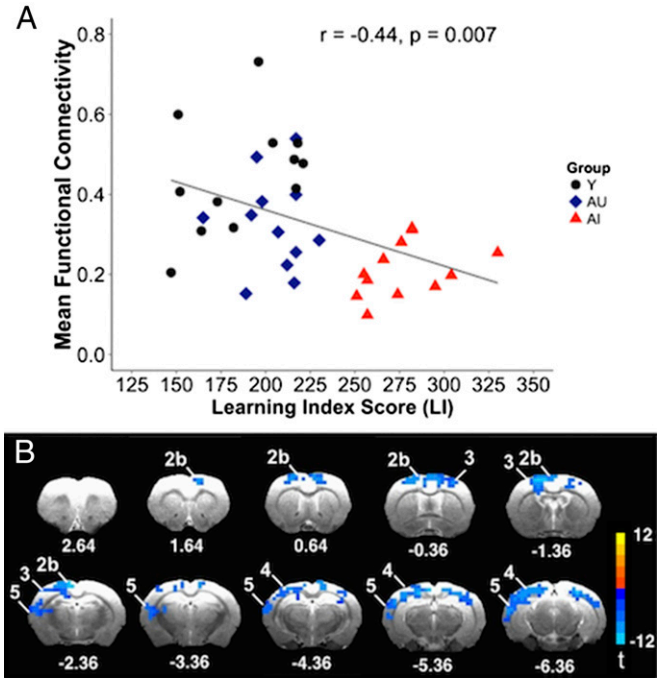

Fig. 5. Results from a linear regression showing (*A*) scatterplot of the correlation between mean functional connectivity with the RSC/PCC and spatial memory performance (LI score) for all Y (black circle), AU (blue diamond), or AI (red triangle) rats; and (*B*) the distribution of regions showing significant associations ($P < 0.05$, corrected for multiple comparisons). Although poor spatial learning was associated with low FC across a variety of regions that displayed significant functional connectivity reductions in the AI group, correlations computed for each group considered separately were not statistically significant. Fig. 4 shows key. Coordinates represent distance relative to bregma (in milliliters).

Discussion

Mapping the borders between brain aging and neurodegeneration has proved challenging on the basis of human research. In the current study, aged rats with impaired memory exhibited a distinct network signature, characterized by widely distributed, marked reductions in temporally coherent rs-FC with the RSC/PCC. By comparison, successful cognitive aging, among aged rats with preserved spatial memory, was associated with a qualitatively different pattern comprising reduced connectivity in a network that showed anticorrelated activity with the RSC/PCC in young adults. The implications of these findings are elaborated below, including the concept that rs-network disruption associated with cognitive decline reflects a unique neurobiological condition of aging permissive for the development of neurodegeneration, and the related idea that optimally healthy cognitive aging is enabled by an active neuroadaptive trajectory.

A key finding from this study is that disrupted cortical network connectivity is not an inevitable consequence of aging and that changes in rs-FC with the RSC/PCC hub are linked instead to compromised integrity of the hippocampal system. Although the findings reported here are not selective for the DMN, they parallel human studies demonstrating that the degree of temporal coupling between cortical and hippocampal DMN nodes in aging is associated with performance on tests of episodic memory (12, 44). Considerable interest has centered on the network mechanisms that mediate this association. In a recent study, Salami et al. (44) reported that older, cognitively normal participants with increased FC between the left and right hippocampus exhibit a loss of associated FC along the anterior–posterior axis of the DMN, concomitant with poor episodic memory. The proposed account of these findings is that increased interhemispheric temporal coherence in the hippocampus disrupts interactions with neocortical components of a network critical for normal memory. This interpretation is compatible with an "activity-dependent degeneration" model in which exuberant connectivity and excess neural activity in aging comprise a required permissive condition for the development and spread of neuropathology, and for consequent network dysconnectivity (45, 46). Support for this model includes evidence documenting hyperactivity and increased connectivity in mild cognitive impairment (MCI), preceding the dramatic reductions in whole-brain activity observed with the progression to AD (47, 48).

There is substantial precedent for the idea that excessive neural activity is a prominent feature of neurocognitive impairment in both the rat model used here and human aging. Whether changes in activity are compensatory or a driver of impairment, however, is less clear. Key findings in this context include the observation that, relative to young adults and aged unimpaired animals, aged rats with memory deficits exhibit significantly increased baseline firing rates in the hippocampus (49). Pharmacological treatments that dampen this excess activity (e.g., low-dose administration of the antiepileptic drug levetiracetam) rescue memory, suggesting that these neurophysiological and cognitive signatures of hippocampal aging are causally related (50). Human fMRI studies, founded in part on this preclinical animal work, have documented elevated activity in the hippocampus of older subjects with corresponding memory deficits (51). Moreover, both effects are reversed by the same pharmacological intervention that proved beneficial in aged rats (52). Aberrant neural activity is directly implicated in amyloid beta processing and release in neural circuitry affected early and severely in the course of AD (53), and the magnitude of amyloid deposition in key DMN hubs is coupled with changes in cortical rs-dynamics (54). Recent evidence also indicates that soluble amyloid beta oligomer delivery both increases neuronal activity and blunts memory-related synaptic plasticity in the hippocampus (i.e., long-term potentiation), and that these effects are reversed by pharmacological treatments that restore normal neuronal excitability (55). Taken together, these findings raise the possibility that the changes in FC documented here may comprise neural network consequences of distributed changes in excitatory/inhibitory balance, and a signature of the neurobiological condition that renders cognitive aging the primary risk for neurodegenerative disease.

The testable prediction based on this proposal is that interventions that normalize excitability and improve memory in AI animals will rescue rs-FC in this model.

In addition to a focus on impairment, there is considerable interest in identifying the neurobiological substrates that support preserved cognitive function during aging. Anticorrelated networks display inversely correlated rs-activity patterns across brain regions, and, whereas there is little consensus concerning their functional significance, current proposals suggest a role in switching between alternate modes of information processing (3). For example, the allocation of attentional resources toward external stimuli is associated with engagement of both the central executive (CENs) and salience networks (SNs), concurrent with deactivations in the DMN (40, 41, 56). Evidence suggests that the frontal insular (FIC) and anterior cingulate cortices (ACCs), key nodes in the SN, operate as a control system, determining which network, the DMN or CEN, should be most engaged at any given time (41). In the current study, significant changes in FC in aged rats with preserved cognitive function were restricted to an anticorrelated network observed in young rats that involved the ACC and FIC. This pattern of results is reminiscent of other recent observations in this model, using in situ hybridization for the plasticity-related immediate gene Arc to map the distribution of regional activations induced during behavioral testing (57). In that investigation, a task that emphasized rapid switching between spatial and nonspatial response strategies was associated with Arc induction selectively in the prefrontal cortex (PFC) in both Y and AI rats. PFC Arc expression in aged rats with preserved spatial memory, in comparison, was completely unaffected by demands on cognitive flexibility, as though top-down control over the balance between competing memory systems is reduced in AU rats (57).

The present findings extend these observations, demonstrating at a functional neural network level that successful cognitive aging is associated with significant neuroadaptation, rather than compensation, reserve, or simply the persistence of a more youthful phenotype. The development of interventions to promote neuroadaptive trajectories, advantaging the capacity of the adult brain for plastic reorganization, represents an alternative to current strategies, toward bending the course of aging away from neurodegeneration.

Materials and Methods

Subjects. Young adult (6–8 mo; $n = 12$) and aged (24–26 mo; $n = 24$) male Long–Evans rats (Charles River Laboratories) were individually housed and maintained under specific pathogen-free conditions on a 12-h light/dark cycle at the National Institute on Aging/National Institute on Drug Abuse (NIA/NIDA) animal facilities in the Biomedical Research Center (Baltimore, MD). Standard rat chow and water were available ad libitum throughout the experiments.

Experimental Design. Animals were first trained in the Morris water maze (MWM) and then transferred to an adjacent vivarium and imaging facilities at NIDA. After an acclimation period of 1 mo, rs-fMRI data were acquired, and repeated only in cases where postacquisition quality-control assessment or physiological monitoring revealed poor data quality from the initial scan. All procedures were approved by the NIA and NIDA Intramural Research Programs' Institutional Animal Care and Use Committees, in accordance with the National Research Council Guide for the Care and Use of Laboratory Animals.

MWM Task. Hippocampal spatial learning and memory were assessed using a standardized version of the MWM described in detail elsewhere (37) (*SI Materials and Methods* shows details).

Resting-State fMRI Procedure.

Anesthesia and physiology. Animals were placed in a chamber with 2% iso in oxygen and air (1:1), followed by an initial s.c. injection of the α2 adrenergic agonist dex (0.015 mg/kg). The bolus dose of dex enabled positioning in a customized MRI cradle equipped with a nose cone and incisor bar, allowing for head fixation and iso/oxygen delivery. Anesthesia was then maintained throughout scanning with dex (0.01 mg/kg/hr) delivered via a catheter (s.c.), plus iso in oxygen-rich air (30% or greater) through the nose cone. Iso was set initially at 2% for the anatomical scans, and subsequently reduced to a target range of 0.5–0.75% before the start of rs-fMRI scanning (~2 h from the bolus dex injection). The iso was titrated to maintain normal physiology (*SI Materials and Methods* shows details).

A pulse oximeter (Mouse OxPlus, Starr Life Sciences) was attached to the left hind paw to measure heart rate and arterial oxygen concentration (O_2 saturation range: 95–100%). Respiration rate was measured during rs-fMRI scanning with a sensor placed under the animal's chest. Core body temperature was measured using a rectal thermometer and maintained at 37.2 ± 0.5 °C using a circulating water blanket.

Scanning protocol. The fMRI experiments were performed on a Bruker Biospin 9.4T scanner (Bruker Medizintechnik). A volume coil was used for radio frequency excitation and a single loop circular surface coil for signal reception. High-resolution T2-weighted anatomical images were acquired first, using a rapid acquisition with relaxation enhancement (RARE) sequence [repetition time (TR) = 2,000 ms, effective echo time (TE) = 50 ms, RARE factor = 8]. The decussation of the anterior commissure (–0.36 mm from bregma) was clearly distinguished in T2-weighted images and was used as a fiducial to localize slice acquisitions. Functional scanning began approximately 2 h after the initial dex injection, based on previous findings that the rs-BOLD signal, as well as heart and respiration rates, stabilize after this time point (24).

Functional scans were acquired using a single-shot gradient-echo echo-planar imaging (EPI) sequence. Scan parameters were as follows: field of view (FOV) = 3.5 cm, matrix size = 64 × 64, TE = 15 ms, and TR = 1,000 ms, 15 slices with a thickness of 1 mm, 300 volumes per session. Three to five sequential 5-min rs-fMRI scans were collected per session, depending on the length of time the animal remained physiologically stable and lightly anesthetized.

Preprocessing steps. Geometric distortions in EPI images were corrected using the phase labeling for additional coordinate encoding (PLACE) method (58). All preprocessing steps were performed within the Analysis of Functional Neuroimages (AFNI) framework (59), except for independent component analysis (ICA), which was performed using the FMRIB Software Library (FSL) (60). Data preprocessing steps included: (*i*) skull-stripping the anatomical T2 scans (3dAutomask, AFNI), coregistration with their corresponding functional scans, followed by merging all images onto a common 3D space using a size-matched aged animal as reference; (*ii*) removing the first five volumes of each fMRI time series because the magnetization had not reached a steady state when acquiring these volumes (3dcalc, AFNI); (*iii*) single-subject ICA to remove noise components (Melodic, FSL); (*iv*) slice-time correction for interleaved ascending slice acquisition (3dTshift, AFNI); (*v*) linear and quadratic trend removal (3dDetrend, AFNI); (*vi*) band-pass temporal filtering (0.01–0.1 Hz) (3dFourier, AFNI); and (*vii*) spatial smoothing with a Gaussian kernel (full width at half maximum = 0.6 mm, 3dmerge with the –blur option, AFNI). For step *iii*, single subject ICA was conducted by a single rater blind to the subjects' group identity, with no significant between-group differences in the number of ICA components removed (Kruskal–Wallis test, $H = 1.047$, df = 2, $P = 0.593$). Brain masks were then created for each subject that excluded the ventricles, white matter, and nonbrain tissue from further analysis.

Data analysis. Whole-brain FC maps were constructed for each animal by placing a 13-voxel seed in the RSC/PCC using coordinates from previous research (24) (Fig. 2, *Bottom Right*) and computing the resulting Pearson's correlation coefficients between the mean time course of the seed and every other voxel in the brain (*SI Materials and Methods* shows details). The resulting FC maps were transformed using Fisher's z to yield normally distributed data and averaged per animal for use in subsequent analyses.

A one-way ANOVA (3dANOVA, AFNI) was used to compare FC maps between the Y, AU, and AI groups ($n = 12$ per group). There was an a priori interest in all between-group comparisons (Y vs. AU, Y vs. AI, and AU vs. AI). Activity was considered significant at $P < 0.05$, corrected for multiple comparisons using an uncorrected $P < 0.01$, cluster size = 9, $t \geq 2.82$ (determined using 3dClustSim in AFNI). A linear regression model was used (3dRegAna, AFNI) to determine the relationship, on a voxel-wise basis, between LI scores (as a measure of hippocampal memory capacity) and FC using the RSC/PCC seed. Voxels with $P < 0.05$, corrected for multiple comparisons, were considered significant.

As a negative control, we conducted a parallel analysis using a seed positioned in the PC. Procedures essentially identical to those above were used to create and compare FC maps using the PC seed.

Group differences in physiology measures were analyzed using a nonparametric Kruskal–Wallis or Mann–Whitney test. A one-way ANOVA was used to evaluate group differences in body weight.

ACKNOWLEDGMENTS. This work was supported by the Intramural Research Programs of the NIH's National Institute on Aging and National Institute on Drug Abuse.

1. Raichle ME, et al. (2001) A default mode of brain function. *Proc Natl Acad Sci USA* 98(2): 676–682.
2. Greicius MD, Krasnow B, Reiss AL, Menon V (2003) Functional connectivity in the resting brain: A network analysis of the default mode hypothesis. *Proc Natl Acad Sci USA* 100(1): 253–258.
3. Buckner RL, Andrews-Hanna JR, Schacter DL (2008) The brain's default network: Anatomy, function, and relevance to disease. *Ann N Y Acad Sci* 1124:1–38.
4. Biswal B, Yetkin FZ, Haughton VM, Hyde JS (1995) Functional connectivity in the motor cortex of resting human brain using echo-planar MRI. *Magn Reson Med* 34(4):537–541.
5. Hampson M, Driesen NR, Skudlarski P, Gore JC, Constable RT (2006) Brain connectivity related to working memory performance. *J Neurosci* 26(51):13338–13343.
6. Seeley WW, et al. (2007) Dissociable intrinsic connectivity networks for salience processing and executive control. *J Neurosci* 27(9):2349–2356.
7. Andrews-Hanna JR, et al. (2007) Disruption of large-scale brain systems in advanced aging. *Neuron* 56(5):924–935.
8. Damoiseaux JS, et al. (2008) Reduced resting-state brain activity in the "default network" in normal aging. *Cereb Cortex* 18(8):1856–1864.
9. Sambataro F, et al. (2010) Age-related alterations in default mode network: Impact on working memory performance. *Neurobiol Aging* 31(5):839–852.
10. Mevel K, et al. (2013) Age effect on the default mode network, inner thoughts, and cognitive abilities. *Neurobiol Aging* 34(4):1292–1301.
11. He J, et al. (2012) Influence of functional connectivity and structural MRI measures on episodic memory. *Neurobiol Aging* 33(11):2612–2620.
12. Wang L, et al. (2010) Intrinsic connectivity between the hippocampus and posteromedial cortex predicts memory performance in cognitively intact older individuals. *Neuroimage* 51(2):910–917.
13. Whitfield-Gabrieli S, Ford JM (2012) Default mode network activity and connectivity in psychopathology. *Annu Rev Clin Psychol* 8:49–76.
14. Greicius MD, Srivastava G, Reiss AL, Menon V (2004) Default-mode network activity distinguishes Alzheimer's disease from healthy aging: Evidence from functional MRI. *Proc Natl Acad Sci USA* 101(13):4637–4642.
15. Damoiseaux JS, Prater KE, Miller BL, Greicius MD (2012) Functional connectivity tracks clinical deterioration in Alzheimer's disease. *Neurobiol Aging* 33(4):828.e19–828.e30.
16. Brier MR, et al. (2012) Loss of intranetwork and internetwork resting state functional connections with Alzheimer's disease progression. *J Neurosci* 32(26):8890–8899.
17. Buckner RL, et al. (2005) Molecular, structural, and functional characterization of Alzheimer's disease: Evidence for a relationship between default activity, amyloid, and memory. *J Neurosci* 25(34):7709–7717.
18. Buckner RL, et al. (2009) Cortical hubs revealed by intrinsic functional connectivity: Mapping, assessment of stability, and relation to Alzheimer's disease. *J Neurosci* 29(6): 1860–1873.
19. Hedden T, et al. (2009) Disruption of functional connectivity in clinically normal older adults harboring amyloid burden. *J Neurosci* 29(40):12686–12694.
20. Mormino EC, et al. (2011) Relationships between β-amyloid and functional connectivity in different components of the default mode network in aging. *Cereb Cortex* 21(10): 2399–2407.
21. Drzezga A, et al. (2011) Neuronal dysfunction and disconnection of cortical hubs in non-demented subjects with elevated amyloid burden. *Brain* 134(Pt 6):1635–1646.
22. Sheline YI, et al. (2010) Amyloid plaques disrupt resting state default mode network connectivity in cognitively normal elderly. *Biol Psychiatry* 67(6):584–587.
23. Jack CR, Jr, et al. (2012) An operational approach to National Institute on Aging-Alzheimer's Association criteria for preclinical Alzheimer disease. *Ann Neurol* 71(6): 765–775.
24. Lu H, et al. (2012) Rat brains also have a default mode network. *Proc Natl Acad Sci USA* 109(10):3979–3984.
25. Schwarz AJ, et al. (2013) Anti-correlated cortical networks of intrinsic connectivity in the rat brain. *Brain Connect* 3(5):503–511.
26. Vincent JL, et al. (2007) Intrinsic functional architecture in the anaesthetized monkey brain. *Nature* 447(7140):83–86.
27. Rilling JK, et al. (2007) A comparison of resting-state brain activity in humans and chimpanzees. *Proc Natl Acad Sci USA* 104(43):17146–17151.
28. Mantini D, et al. (2011) Default mode of brain function in monkeys. *J Neurosci* 31(36): 12954–12962.
29. Hutchison RM, Everling S (2012) Monkey in the middle: Why non-human primates are needed to bridge the gap in resting-state investigations. *Front Neuroanat* 6:29.
30. Fletcher BR, Rapp PR (2012) Normal neurocognitive aging. *Handbook of Psychology*, ed Weiner IB (Wiley, New York), 2nd Ed, pp 643–664.
31. Pawela CP, et al. (2008) Resting-state functional connectivity of the rat brain. *Magn Reson Med* 59(5):1021–1029.
32. Nasrallah FA, Lew SK, Low AS, Chuang KH (2014) Neural correlate of resting-state functional connectivity under α2 adrenergic receptor agonist, medetomidine. *Neuroimage* 84:27–34.
33. Stafford JM, et al. (2014) Large-scale topology and the default mode network in the mouse connectome. *Proc Natl Acad Sci USA* 111(52):18745–18750.
34. Prince M, et al. (2013) The global prevalence of dementia: A systematic review and metaanalysis. *Alzheimers Dement* 9(1):63–75.e2.
35. Draganski B, Lutti A, Kherif F (2013) Impact of brain aging and neurodegeneration on cognition: evidence from MRI. *Curr Opin Neurol* 26(6):640–645.
36. Jagust W (2013) Vulnerable neural systems and the borderland of brain aging and neurodegeneration. *Neuron* 77(2):219–234.
37. Gallagher M, Burwell R, Burchinal M (1993) Severity of spatial learning impairment in aging: Development of a learning index for performance in the Morris water maze. *Behav Neurosci* 107(4):618–626.
38. Tomás Pereira I, et al. (2013) CREB-binding protein levels in the rat hippocampus fail to predict chronological or cognitive aging. *Neurobiol Aging* 34(3):832–844.
39. Torrealba F, Valdés JL (2008) The parietal association cortex of the rat. *Biol Res* 41(4): 369–377.
40. Fox MD, et al. (2005) The human brain is intrinsically organized into dynamic, anticorrelated functional networks. *Proc Natl Acad Sci USA* 102(27):9673–9678.
41. Sridharan D, Levitin DJ, Menon V (2008) A critical role for the right fronto-insular cortex in switching between central-executive and default-mode networks. *Proc Natl Acad Sci USA* 105(34):12569–12574.
42. Gallagher M, et al. (2006) Individual differences in neurocognitive aging of the medial temporal lobe. *Age (Dordr)* 28(3):221–233.
43. Curcio CA, McNelly NA, Hinds JW (1985) Aging in the rat olfactory system: Relative stability of piriform cortex contrasts with changes in olfactory bulb and olfactory epithelium. *J Comp Neurol* 235(4):519–528.
44. Salami A, Pudas S, Nyberg L (2014) Elevated hippocampal resting-state connectivity underlies deficient neurocognitive function in aging. *Proc Natl Acad Sci USA* 111(49): 17654–17659.
45. de Haan W, Mott K, van Straaten EC, Scheltens P, Stam CJ (2012) Activity dependent degeneration explains hub vulnerability in Alzheimer's disease. *PLOS Comput Biol* 8(8):e1002582.
46. Palop JJ, Mucke L (2010) Amyloid-beta-induced neuronal dysfunction in Alzheimer's disease: From synapses toward neural networks. *Nat Neurosci* 13(7):812–818.
47. Celone KA, et al. (2006) Alterations in memory networks in mild cognitive impairment and Alzheimer's disease: An independent component analysis. *J Neurosci* 26(40): 10222–10231.
48. Dickerson BC, et al. (2005) Increased hippocampal activation in mild cognitive impairment compared to normal aging and AD. *Neurology* 65(3):404–411.
49. Wilson IA, Gallagher M, Eichenbaum H, Tanila H (2006) Neurocognitive aging: Prior memories hinder new hippocampal encoding. *Trends Neurosci* 29(12):662–670.
50. Koh MT, Haberman RP, Foti S, McCown TJ, Gallagher M (2010) Treatment strategies targeting excess hippocampal activity benefit aged rats with cognitive impairment. *Neuropsychopharmacology* 35(4):1016–1025.
51. Yassa MA, et al. (2010) High-resolution structural and functional MRI of hippocampal CA3 and dentate gyrus in patients with amnestic mild cognitive impairment. *Neuroimage* 51(3):1242–1252.
52. Bakker A, et al. (2012) Reduction of hippocampal hyperactivity improves cognition in amnestic mild cognitive impairment. *Neuron* 74(3):467–474.
53. Jagust WJ, Mormino EC (2011) Lifespan brain activity, β-amyloid, and Alzheimer's disease. *Trends Cogn Sci* 15(11):520–526.
54. Sperling RA, et al. (2009) Amyloid deposition is associated with impaired default network function in older persons without dementia. *Neuron* 63(2):178–188.
55. Lei M, et al. (2016) Soluble Aβ oligomers impair hippocampal LTP by disrupting glutamatergic/GABAergic balance. *Neurobiol Dis* 85:111–121.
56. Fransson P (2006) How default is the default mode of brain function? Further evidence from intrinsic BOLD signal fluctuations. *Neuropsychologia* 44(14):2836–2845.
57. Tomás Pereira I, Gallagher M, Rapp PR (2015) Head west or left, east or right: Interactions between memory systems in neurocognitive aging. *Neurobiol Aging* 36(11): 3067–3078.
58. Xiang QS, Ye FQ (2007) Correction for geometric distortion and N/2 ghosting in EPI by phase labeling for additional coordinate encoding (PLACE). *Magn Reson Med* 57(4): 731–741.
59. Cox RW (1996) AFNI: Software for analysis and visualization of functional magnetic resonance neuroimages. *Comput Biomed Res* 29(3):162–173.
60. Beckmann CF, DeLuca M, Devlin JT, Smith SM (2005) Investigations into resting-state connectivity using independent component analysis. *Philos Trans R Soc Lond B Biol Sci* 360(1457):1001–1013.
61. Spiegel AM, Koh MT, Vogt NM, Rapp PR, Gallagher M (2013) Hilar interneuron vulnerability distinguishes aged rats with memory impairment. *J Comp Neurol* 521(15):3508–3523.
62. Williams KA, et al. (2010) Comparison of alpha-chloralose, medetomidine and isoflurane anesthesia for functional connectivity mapping in the rat. *Magn Reson Imaging* 28(7):995–1003.
63. Grandjean J, Schroeter A, Batata I, Rudin M (2014) Optimization of anesthesia protocol for resting-state fMRI in mice based on differential effects of anesthetics on functional connectivity patterns. *Neuroimage* 102(Pt 2):838–847.
64. Shen J, et al. (2013) MR volumetric study of piriform-cortical amygdala and orbitofrontal cortices: The aging effect. *PLoS One* 8(9):e74526.
65. Datiche F, Cattarelli M (1996) Reciprocal and topographic connections between the piriform and prefrontal cortices in the rat: A tracing study using the B subunit of the cholera toxin. *Brain Res Bull* 41(6):391–398.